Winter 1-13-2015

Recent origin of low trabecular bone density in modern humans

Habiba Chirchir PhD
Marshall University, chirchir@marshall.edu

Tracy L. Kivell

Christopher B. Ruff

Jean-Jacques Hublin

Kristian J. Carlson

See next page for additional authors

Recommended Citation

Chirchir H, Kivell TL, Ruff CB, Hublin JJ, Carlson KJ, Zipfel B, Richmond BG (2015) Recent origin of low trabecular bone density in modern humans. Proceedings of the National Academy of Sciences 112(2):366-71.

Authors
Habiba Chirchir PhD, Tracy L. Kivell, Christopher B. Ruff, Jean-Jacques Hublin, Kristian J. Carlson, Bernhard Zipfel, and Brian G. Richmond

Recent origin of low trabecular bone density in modern humans

Habiba Chirchir[a,b,1], Tracy L. Kivell[c,d], Christopher B. Ruff[e], Jean-Jacques Hublin[d], Kristian J. Carlson[f,g], Bernhard Zipfel[f], and Brian G. Richmond[a,b,h,1]

[a]Center for the Advanced Study of Hominid Paleobiology, Department of Anthropology, The George Washington University, Washington, DC 20052; [b]Human Origins Program, Department of Anthropology, National Museum of Natural History, Smithsonian Institution, Washington, DC 20560; [c]Animal Postcranial Evolution Laboratory, School of Anthropology and Conservation, University of Kent, Canterbury, Kent, CT2 7NR, United Kingdom; [d]Department of Human Evolution, Max Planck Institute for Evolutionary Anthropology, D-04103 Leipzig, Germany; [e]Center for Functional Anatomy and Evolution, Johns Hopkins University School of Medicine, Baltimore, MD 21205; [f]Evolutionary Studies Institute, The University of the Witwatersrand, Braamfontein 2000 Johannesburg, South Africa; [g]Department of Anthropology, Indiana University, Bloomington, IN 47405; and [h]Division of Anthropology, American Museum of Natural History, New York, NY 10024

Edited by Erik Trinkaus, Washington University, St. Louis, MO, and approved November 26, 2014 (received for review June 23, 2014)

Humans are unique, compared with our closest living relatives (chimpanzees) and early fossil hominins, in having an enlarged body size and lower limb joint surfaces in combination with a relatively gracile skeleton (i.e., lower bone mass for our body size). Some analyses have observed that in at least a few anatomical regions modern humans today appear to have relatively low trabecular density, but little is known about how that density varies throughout the human skeleton and across species or how and when the present trabecular patterns emerged over the course of human evolution. Here, we test the hypotheses that (*i*) recent modern humans have low trabecular density throughout the upper and lower limbs compared with other primate taxa and (*ii*) the reduction in trabecular density first occurred in early *Homo erectus*, consistent with the shift toward a modern human locomotor anatomy, or more recently in concert with diaphyseal gracilization in Holocene humans. We used peripheral quantitative CT and microtomography to measure trabecular bone of limb epiphyses (long bone articular ends) in modern humans and chimpanzees and in fossil hominins attributed to *Australopithecus africanus*, *Paranthropus robustus*/early *Homo* from Swartkrans, *Homo neanderthalensis*, and early *Homo sapiens*. Results show that only recent modern humans have low trabecular density throughout the limb joints. Extinct hominins, including pre-Holocene *Homo sapiens*, retain the high levels seen in nonhuman primates. Thus, the low trabecular density of the recent modern human skeleton evolved late in our evolutionary history, potentially resulting from increased sedentism and reliance on technological and cultural innovations.

trabecular bone | human evolution | gracilization | *Homo sapiens* | sedentism

Obligate bipedalism—a defining feature of humans that distinguishes us from our closest living relatives, the African apes—has transformed the human skeleton. Among these unique features are long lower limbs with large joint surfaces. These large joint surfaces help distribute loads over a larger surface area and thus are better at resisting the high forces incurred during locomotion on two limbs instead of four (1–5). Early African *Homo erectus* at 1.8–1.5 Ma had enlarged lower limb joint surfaces (1, 3) and a larger stature (6) and body mass (7, 8) than many earlier hominins, and this pattern often is considered to reflect the emergence of a more modern human-like body plan (1, 3, 5, 6, 9; but also see ref. 7).

Recent modern human (Holocene *Homo sapiens*) skeletons also appear to be gracile as compared with earlier hominins (10–14). Here, "gracilization" refers to the reduction in strength and bone mass relative to body mass inferred from osseous tissue and overall bone size and has been studied mainly using diaphyseal cortical bone cross-sections (10–16). Although the relationship between mechanical loading during life and bone strength is likely to be complex (17), there is much evidence that increased mechanical loading leads to increases in relative bone strength (18). Thus, diaphyseal skeletal gracilization in recent modern humans relative to earlier hominins generally has been attributed to a decrease in daily physical activity via technological and cultural innovations (6, 10, 13–15, 19–22).

There also is evidence that increased activity level and mechanical loading increases trabecular bone mineral density within limb bones (ref. 23 and references therein). However, although there currently is extensive literature on the variation and evolution of long bone shaft strength in humans and fossil hominins (10, 15, 16, 24–27), there has been comparatively less research on trabecular bone (28–30) because of the technical challenges in quantifying its structure: limited access to high-resolution CT (microCT), problems with preservation and/or imaging of fine trabecular structures, particularly in fossils, and intensive processing time. A few studies examining individual limb elements have reported low trabecular density, as measured by volumetric density (the trabecular bone fraction, TBF, or bone volume relative to total volume), in recent modern human epiphyses. The recent modern human arm (humerus) and hand (metacarpals) have low TBF (31, 32) and mineral density (33) compared with chimpanzees and orangutans. This finding might be expected, because humans rarely use their upper limbs for locomotion and therefore do not habitually expose their upper limb bones to the high loads of body-weight support. Indeed, recent modern human upper limb bones have relatively low diaphyseal strengths compared with the lower limbs (34). However, recent modern humans also have low TBF in the calcaneus (35) and metatarsals (36) compared with great apes, despite the increased proportionate loading and full body-weight support incurred during bipedal locomotion.

To our knowledge, this study is the first to examine how trabecular density varies throughout the human appendicular skeleton, how that variation compares with other primates, and how trabecular

Significance

The human skeleton is unique in having low trabecular density representing a lightly built human body form. However, it remains unknown when during human evolution this unique characteristic first appeared. To our knowledge, this study is the first to examine trabecular bone density throughout the skeleton of fossil hominins spanning several million years. The results show that trabecular density remained high throughout human evolution until it decreased significantly in recent modern humans, suggesting a possible link between changes in our skeleton and increased sedentism.

Author contributions: H.C. and B.G.R. designed research; H.C. performed research; T.L.K., C.B.R., J.-J.H., K.J.C., and B.Z. contributed new reagents/analytic tools; H.C. analyzed data; H.C. wrote the paper; and T.L.K., C.B.R., and B.G.R. contributed to writing the paper.

The authors declare no conflict of interest.

This article is a PNAS Direct Submission.

[1]To whom correspondence may be addressed. Email: habibachirchir@gmail.com or brichmond@amnh.org.

This article contains supporting information online at www.pnas.org/lookup/suppl/doi:10.1073/pnas.1411696112/-/DCSupplemental.

Table 1. Sample size of taxa studied

Taxon	Proximal humerus	Proximal ulna	Distal radius	Distal metacarpal	Proximal femur	Distal tibia	Distal metatarsal
Homo sapiens	38	38	38	30	38	38	35
Pan troglodytes	17	17	17	17	17	17	17
Pongo pygmaeus	15	16	16	16	16	16	16
Papio anubis	17	17	17	12	18	18	17
Australopithecus sp.	—	—	—	—	1	—	—
Australopithecus africanus	1	4	—	5	3	3	—
Paranthropus robustus/early *Homo*	—	—	1	2	—	—	2
Homo neanderthalensis	3	2	2	1	1	—	—
Early *Homo sapiens*	1	1	—	2	2	2	2

See Table S1 for a breakdown of each sex included in the extant samples and Table S2 for a complete list of the specimens included in each fossil taxon.

density evolved in the hominin lineage. We test the hypotheses that (*i*) recent modern humans have lower TBF throughout the upper and lower limbs compared with that of other primates and (*ii*) the reduction in TBF first occurred in African *Homo erectus*, consistent with the shift toward a modern human locomotor anatomy, or more recently in concert with diaphyseal gracilization in recent modern humans. This study is the first, to our knowledge, to evaluate TBF in upper and lower limb joints in fossil hominins from late Pliocene *Australopithecus* to recent *Homo*.

To assess whether low trabecular density is a systemic phenomenon throughout the human skeleton, we examined trabecular density in seven epiphyseal elements throughout the upper limb (humeral head, proximal ulna, distal radius, metacarpal heads) and lower limb (femoral head, distal tibia, and metatarsal heads) (Table 1 and Tables S1 and S2). We measured trabecular density in a 2D image as the ratio of bone pixels/total pixels (i.e., the TBF) within a defined region of interest (ROI) for each epiphysis (Fig. S1). We first compared TBF across extant primate (baboon, orangutan, chimpanzee, and recent modern human) limb epiphyses (Table 1 and Table S2). We also compared TBF in late Pliocene and Pleistocene hominins ($n = 42$) within the context of changes in body form in early *Homo* at 1.8 Ma and throughout the Pleistocene (Table 1 and Table S2).

Results

Recent Modern Human Trabecular Density. Results show that the TBF is lower in recent modern humans than in the other primate taxa examined, including in lower limb joints that might be expected to have greater TBF in committed bipeds who bear comparatively more body weight through these limbs (Figs. 1 and 2). ANOVA with Tukey post hoc pairwise comparisons shows that recent modern human upper and lower limb joints have significantly ($P < 0.001$) lower TBF than all other primates (Fig. 2 and Table S3), albeit with some variation in values across elements (Fig. 3). Pooled data for all upper limb elements for each taxon indicate that baboons have the greatest TBF, and recent modern humans exhibit the least (Fig. 2*A*). Although there is some overlap in TBF between recent modern humans and chimpanzees, humans have systematically lower TBF in every anatomical element sampled (Fig. 3*A* and Table 2). Within lower limbs, the pooled results again reveal that the TBF is significantly ($P < 0.001$) lower in recent modern human epiphyses than in all other primate taxa (Fig. 2*B*). Relative to the upper limb, the TBF values of individual elements in the lower limb show an even greater separation between recent modern humans and chimpanzees (Fig. 3*B*).

Fossil Hominin TBF. In the upper limb, the mean TBF of the humeral head in all pre-Holocene fossil hominins falls more than 2 SDs above the recent modern human mean (Fig. 3*A* and Table 2). In particular, the *Australopithecus africanus* humeral head has the highest TBF values of the taxa examined, having a substantially higher TBF than chimpanzee humeri and far greater (9 SDs) TBF values than the humeri of recent modern humans. Neanderthal and early modern human humeral TBF values are intermediate between those of chimpanzees and recent modern humans (Table 2).

The proximal ulna TBF is high in fossil hominins. *A. africanus* and Neanderthal mean TBF values are 4 SDs above the recent modern human mean. The early modern (i.e., pre-Holocene) human proximal ulna TBF is above the recent modern human mean (1.37 SDs) (Table 2), although it is within the overall range in recent modern humans (Fig. 3). Recent modern humans have a large range of variation, and overall the ulna has the highest TBF of all of the joints in the upper limb (Fig. 3*A* and Table 2). Interestingly, both *A. africanus* and Neanderthals have very a high ulnar TBF, several SDs above the chimpanzee mean (Table 2).

The mean trabecular density for all fossil hominin distal radii, including early *H. sapiens*, is above the recent modern human mean. Means of Neanderthal and Swartkrans specimens (possibly *P. robustus* or early *Homo*) are more than 5 and 2 SDs above the recent modern human mean, respectively, and are comparable to or higher than the mean of chimpanzees (Fig. 3*A* and Table 2). Apart from the Neanderthals, all fossil hominin TBF means for the metacarpal heads are 1 or more SDs above the recent modern human mean (Fig. 3*A* and Table 2). All fossil hominin metacarpal head means fall below the chimpanzee mean. Neanderthal metacarpals stand out in having a low TBF, comparable to that of recent modern humans.

In summary, in terms of TBF, the upper limbs of recent modern humans are lightly built compared with those of pre-Holocene hominins and extant nonhuman primates. A one-way ANOVA between pooled samples of *Australopithecus* and Swartkans upper limb elements vs. fossil *Homo* (including early modern humans) upper limb elements was not significant ($P = 0.17$), but the TBF of recent modern humans was significantly lower than that of fossil *Homo* considered separately ($P < 0.01$) and of all fossil hominins combined ($P < 0.01$) (Table S3).

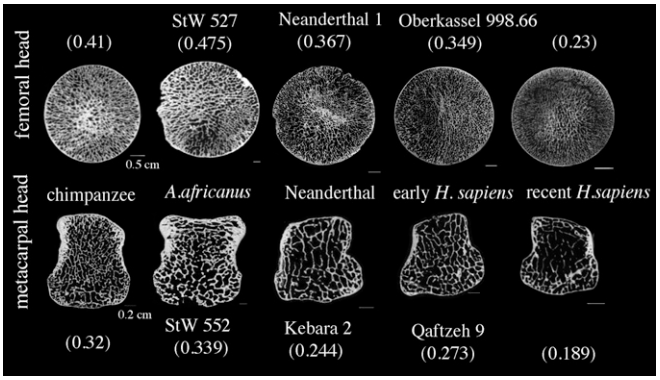

Fig. 1. Proximal femur and distal metacarpal 2D slices of trabecular structure and their associated trabecular fraction values in chimpanzees, recent modern humans, and a sample of fossil taxa demonstrating variation in trabecular fraction across taxa and time.

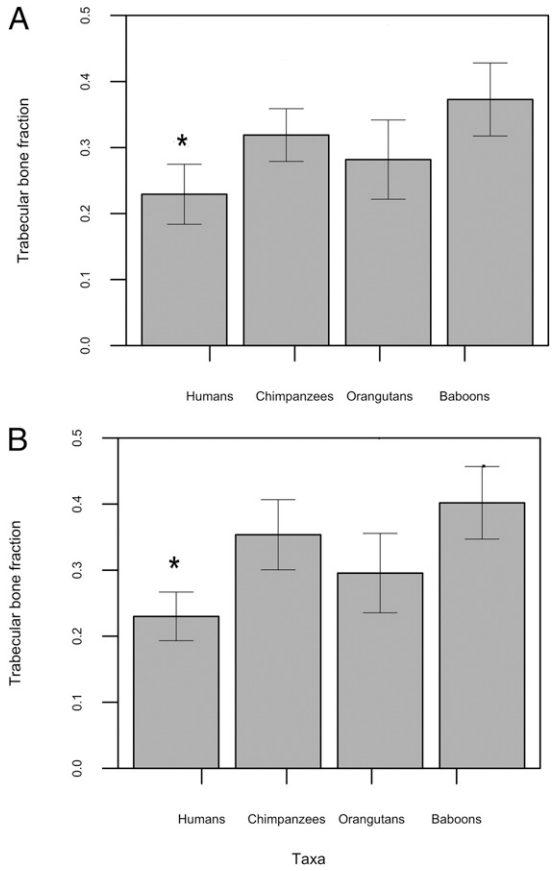

Fig. 2. TBF in upper and lower limb epiphyses in extant taxa. The bar graphs show mean TBF with a 2-SD error bar for all upper limb (*A*) and lower limb (*B*) epiphyses. The asterisk indicates that the trabecular fraction is significantly ($P = 0.001$) lower in recent modern humans than in all other taxa.

In the lower limb, the femoral head TBF of all of the pre-Holocene fossil taxa falls above the observed range for recent modern humans, with fossil group means falling roughly 5 or more SDs above the recent modern human mean (Fig. 3*B* and Table 2). In particular, *A. africanus* femora and the fossil KNM-ER 738 (likely *Paranthropus boisei*, but attribution is uncertain) have TBF values lying more than 7 SDs above the recent modern human mean. In contrast, TBF values of pre-Holocene hominin femora overlap widely with those of chimpanzees, with all group means being within 1 SD of the chimpanzee mean.

Data on the distal tibia show that the mean TBF of *A. africanus* is much higher than that of chimpanzees and is 5 SDs above the mean in recent modern humans (Fig. 3*B* and Table 2). The tibial TBF in early modern humans is intermediate between that of chimpanzees and recent modern humans (Fig. 3*B*).

Results for the metatarsal head indicate that the mean TBF in the two fossil groups—Swartkrans and early modern humans—is more than 3 SDs above the recent modern human mean. Indeed, early modern humans exhibit the greatest mean value across the sample (Fig. 3*B* and Table 2), falling more than 3 SDs above the chimpanzee mean.

In summary, the lower limb pattern shows that recent modern humans have a lower mean TBF than all pre-Holocene hominins, including early modern humans, as well as chimpanzees. Compared with the results for mean upper limb TBF, the lower limbs of recent modern humans have consistently lower TBF values, exhibiting less overlap with any fossil or extant non-human sample. A one-way ANOVA between pooled samples of *Australopithecus* and Swartkrans lower limb elements vs. fossil *Homo* (including early modern humans) lower limb elements was not significantly ($P = 0.18$) different, but the mean TBF in the lower limb elements was significantly lower in recent modern humans than in fossil *Homo* ($P < 0.01$) and was lower than in all fossil hominins combined ($P < 0.01$) (Table S3).

Discussion

Our results show that recent modern humans have low trabecular density, as assessed by TBF, throughout the limb skeleton; the TBF is about 50–75% of that of modern chimpanzees, and some fossil hominins have limb joints more than twice as dense as those of modern humans (Fig. 3). This decrease in trabecular density is a very recent evolutionary phenomenon. Hominins as late as the Late Pleistocene retain high trabecular density (i.e., TBF), suggesting that extant levels of human trabecular density likely emerged in the latest Pleistocene or Holocene. These results support recent studies showing little change in lower limb bone shaft robusticity among *Homo* throughout the Pleistocene, followed by a rapid decrease in recent modern humans in the Holocene (e.g., refs. 11 and 16). Across the sample, the mean trabecular density in all postcranial elements is lower in recent modern humans than in other extant and fossil taxa. In general, *Australopithecus* specimens displayed the greatest trabecular density in the lower limbs, exceeding that in chimpanzees. There is some overlap in the range of trabecular density between early modern humans and Neanderthals, especially in the upper limb. In recent modern humans the range of trabecular density also is closer to that of chimpanzees in the upper limb elements than in the lower limbs (Fig. 3*B*). Thus, although recent modern humans have significantly lower trabecular density in their upper limbs, both the general temporal trend across hominins and the distinctiveness of the low trabecular density in recent modern humans are more marked in the lower limb.

The hypothesis that lower limb trabecular density decreased in early *Homo* in conjunction with the shift toward a more modern human body plan is not supported. We show that both Neanderthals and early modern humans retain high trabecular density

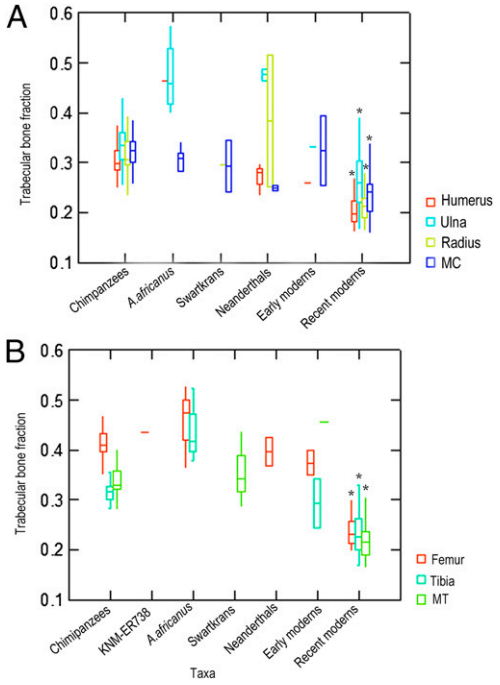

Fig. 3. TBF in each epiphysis across extant and fossil samples. In the box-and-whisker plots the horizontal line shows the median, the box defines the 25th and 75th percentiles, and the whiskers show the range of TBF variation in all upper limb (*A*) and lower limb (*B*) epiphyses. Asterisks indicate that recent modern human values are significantly lower than those of chimpanzees in each epiphyseal element. The Swartkrans sample represents either *P. robustus* or early *Homo*. MC, metacarpal; MT, metatarsal.

Table 2. Mean and SD for each extant and fossil taxon and the number of SDs each fossil sample deviates from the recent human and chimpanzee means, which were treated as reference samples

Element and taxon	Mean trabecular fraction	SD	Mean SDs from recent *Homo sapiens*	Mean SDs from *Pan troglodytes*	Range
Proximal humerus					
Recent *Homo sapiens*	0.20	0.02	—	—	0.16–0.26
Pan troglodytes	0.30	0.03	—	—	0.25–0.37
Australopithecus africanus	0.46	—	9.44	4.79	
Homo neanderthalensis	0.27	—	2.48	−0.95	0.24–0.29
Early *Homo sapiens*	0.26	—	2.10	−1.26	
Proximal ulna					
Recent *Homo sapiens*	0.25	0.05	—	—	0.16–0.39
Pan troglodytes	0.33	0.05	—	—	0.16–0.29
Australopithecus africanus	0.47	—	4.04	2.91	0.40–0.57
Homo neanderthalensis	0.48	—	4.09	2.97	
Early *Homo sapiens*	0.33	—	1.37	−0.11	
Distal radius					
Recent *Homo sapiens*	0.21	0.03	—	—	0.16–0.27
Pan troglodytes	0.31	0.03	—	—	0.23–0.39
Swarkrans	0.30	—	2.55	−0.42	
Homo neanderthalensis	0.38	—	5.30	1.78	
Proximal metacarpal					
Recent *Homo sapiens*	0.23	0.03	—	—	0.16–0.33
Pan troglodytes	0.32	0.03	—	—	0.25–0.38
Australopithecus africanus	0.31	—	1.81	−0.51	0.28–0.33
Paranthropus robustus/early *Homo*	0.29	—	1.47	−0.91	
Homo neanderthalensis	0.25	—	0.29	−2.27	
Early *Homo sapiens*	0.31	—	1.92	−0.38	
Proximal femur					
Recent *Homo sapiens*	0.23	0.02	—	—	0.19–0.29
Pan troglodytes	0.41	0.02	—	—	0.35–0.46
Australopithecus sp.	0.44	—	7.38	0.79	
Australopithecus africanus	0.46	—	8.11	1.48	0.36–0.52
Homo neanderthalensis	0.40	—	5.88	−0.59	
Early *Homo sapiens*	0.37	—	5.10	−1.31	
Distal tibia					
Recent *Homo sapiens*	0.23	0.04	—	—	0.16–0.32
Pan troglodytes	0.31	0.01	—	—	0.28–0.35
Australopithecus africanus	0.44	—	5.03	6.33	0.37–0.52
Early *Homo sapiens*	0.29	—	1.51	−1.10	
Distal metatarsal					
Recent *Homo sapiens*	0.21	0.03	—	—	0.16–0.30
Pan troglodytes	0.34	0.04	—	—	0.26–0.37
Paranthropus robustus/early *Homo*	0.36	—	3.85	0.48	
Early *Homo sapiens*	0.46	—	6.68	3.76	

Positive and negative values refer to the number of SDs above and below the reference sample means, respectively. Ranges are provided only for those samples with $n > 3$.

similar to that in earlier hominins, as compared with the low trabecular density found in recent modern humans. Thus, there is not a consistent, gradual shift toward lighter skeletons during the Pleistocene. On the contrary, our results suggest that there are generally high values, with some variation in skeletal robusticity, throughout the Pleistocene, as also has been observed in shaft strength of limb bones (11, 16, 27).

Similarly, the upper limb elements do not support the hypothesis of a temporal decrease in trabecular density throughout the Pleistocene. Instead, Early Pleistocene and Late Pleistocene taxa all have high trabecular density, supporting the idea that the shift from robust to gracile limbs, even in hands that are used for manipulation rather than for weight-bearing, occurred in the Holocene. Interestingly, the highest TBF values in the upper limb are observed in *A. africanus*, which had the highest lower limb values as well. Samples currently are too small to determine whether *Australopithecus* generally had denser trabecular bone than later hominins, chimpanzees, and other primates, but this observation deserves further attention.

The observation that low trabecular bone density (i.e., TBF) among recent modern humans is more marked in the lower limbs than in the upper limbs may argue for changes in mobility, i.e., increased sedentism, as the primary behavioral event driving skeletal gracilization in the Holocene (11, 15, 21, 37, 38). In addition, some behaviors characteristic of Holocene populations, including nonmechanized agriculture, may involve relatively heavy loading of the upper limbs (e.g., ref. 39) and thus serve to maintain relatively higher trabecular density in those skeletal elements.

Our hypothesis that trabecular density decreases at the same time as diaphyseal gracilization of the skeleton, in conjunction with increasing sedentism in the Holocene, is supported. In many ways, early anatomically modern (Pleistocene) humans were morphologically similar to more recent (Holocene) humans, with more linear bodies, including relatively narrow trunks and reduced mediolateral femoral buttressing (16, 40). Therefore, it is

surprising that early modern humans do not have low trabecular density, as do recent humans, but instead have greater TBF than some of the Early Pleistocene taxa and chimpanzees. Again, these results support the hypothesis that trabecular reorganization occurred only later in human evolutionary history.

The results here imply that the higher trabecular density (i.e., TBF) throughout the skeleton of early modern humans compared with that of recent modern humans may be attributable to greater mechanical loading related to longer travel distances or running in the former. Arguably, the post-Pleistocene reduction in the trabecular density of the upper limb could result, at least in part, from a systemic effect (perhaps metabolic and/or pleiotropic) (41). Therefore it could have been driven indirectly by a decrease in mobility rather than by any specific reduction in upper limb bone loading, e.g., an increase in the use of more sophisticated tools.

A limitation of this study is that it did not assess other trabecular bone architectural parameters, such as trabecular strut anisotropy, thickness, and spacing, which can have significant effects on elastic modulus and strength (42, 43). Anisotropy in particular appears to be related to principal loading direction (42). Work to date suggests that in some anatomical regions, such as metatarsal heads, humans are characterized by higher degrees of anisotropy (36), but in others, such as metacarpal heads, humans and apes have comparable degrees of anisotropy (32). In both these cases, modern human joints are consistently low in TBF (32, 36). Therefore, within specific articulations, it is not clear to what extent parameters such as trabecular anisotropy, thickness, and spacing vary systematically among closely related taxa (32, 36, 44, 45). Incorporating additional structural properties across the same or different anatomical regions in future studies could help determine whether architectural changes (if any) paralleled the changes in trabecular density during hominin evolution and whether they were complementary or compensatory during the transition to recent modern humans.

Also, although mechanical loading can affect trabecular growth (23, 46, 47), direct developmental influences may not account entirely for the marked differences in trabecular density in recent modern humans and pre-Holocene hominins. It is plausible that, as sedentism became prevalent and food sources changed in the Holocene, selection pressure for robust skeletons diminished. In other words, more gracile bodies may have evolved rather than be a product of decreased mechanical stimulus during development. The lack of a significant difference in trabecular density between the (presumably) more active Puye and the industrial-era Terry samples also may argue for longer-term evolutionary as well as direct environmental effects. Moreover, other nonmechanical systemic factors that may influence skeletal morphology, including nutrition and disease prevalence (48, 49), also were affected by the transition to food production and increased sedentism in the Holocene (50, 51).

However, regardless of the proximate mechanisms involved, the reduction of trabecular density observed here among nonforaging Holocene humans relative to all earlier hominins examined and to nonhuman primates is consistent with a reduction in activity level and, in particular, mobility, among very recent human populations.

Materials and Methods

Trabecular density was examined using TBF measured from systematically imaged 2D cross-sectional slices of seven epiphyses throughout the appendicular skeleton: the femoral head, distal tibia, metatarsal head, humeral head, proximal ulna, distal radius, and metacarpal head (Table 1 and Tables S1 and S2).

Samples.

Extant primates. The comparative sample comprises recent modern humans (*Homo sapiens*), chimpanzees (*Pan troglodytes*), orangutans (*Pongo pygmaeus*), and olive baboons (*Papio anubis*) (Table 1 and Table S1). The samples were obtained from the National Museum of Natural History (NMNH), Smithsonian Institution. The nonhuman primates were wild-collected individuals. The recent human sample comprises individuals from the Terry and Puye collections (see *SI Materials and Methods* and Table S4 for more details). Only elements that did not exhibit any pathological signs were selected. Moreover, only adult individuals were selected, based on long bone epiphyseal fusion of all elements and the known ages of the Terry collection. Regarding the Terry collection, specific care was taken to sample individuals under the age of 45 y, mainly to avoid age-related effects (i.e., osteoporosis and osteopenia).

Fossil hominins. The fossil sample included *Australopithecus africanus*, KNM-ER 738 (a femur likely representing *Paranthropus boisei*, but of an uncertain attribution), Swartkrans hominins attributed to either *Paranthropus robustus* or early *Homo*, *Homo neanderthalensis*, and early *Homo sapiens*, using all available postcranial elements from various geographic locations and time periods. However, not all postcranial elements were preserved for each fossil taxon (Table 1 and Table S2; see *SI Materials and Methods* for more details).

CT Data Acquisition. Fossil and extant specimens were CT scanned using two methods, peripheral quantitative CT (pQCT) and microtomography (microCT), because specimen access prevented us from scanning the entire sample with one method. Consequently, to obtain a sufficiently large sample of fossil and extant individuals, trabecular bone was measured in two different ways, and a subsample was measured with both methods. The relationship between the two methods is discussed below.

pQCT data acquisition. 2D slices of extant *H. sapiens*, *P. troglodytes*, *P. pygmaeus*, and *P. anubis* (Table 1 and Table S1) were collected using a pQCT scanner (Stratec Research SA) at the NMNH, Smithsonian Institution. The pQCT scanner measures bone content within a given region; it reports bone mineral density based on the attenuation of X-rays. The raw data represent linear attenuation coefficients, which the pQCT calibrates into hydroxyapatite-equivalent densities, based on a calibration standard (52), and which are reported as density values in milligrams per cubic centimeter. All specimens were scanned at a resolution of 100 μm. Each anatomical element was positioned in a systematic orientation in the pQCT gantry to ensure homologous scanning of the same position and plane through the center of the joint in each specimen (Fig. S2 and see Fig. S4; also see *SI Materials and Methods*).

microCT data acquisition. Like pQCT, microCT imaging relies on the attenuation of X-rays, but the images obtained are reconstructed in 3D. The 2D slices of fossil hominin specimens were derived from high-resolution microCT scans taken in the Department of Human Evolution at the Max Planck Institute for Evolutionary Anthropology (MPI-EVA), Leipzig, Germany, with permission from the respective institutions curating the fossil material (Table S2). All fossil epiphyses were scanned at ∼30 μm using a high-resolution, industrial BIR ACTIS 225/300 microCT scanner.

Four of the fossil specimens studied (Table S2) were affected by the presence of matrix, and therefore segmentation was used to eliminate the matrix. Segmentation identifies the boundary between bone and nonbone and eliminates foreign material that may be present because of the fossilization process. This study used the Ray-casting algorithm method (53) of segmentation because of its reliance on the gray value gradient rather than on absolute gray values. This method was applied to 3D microCT scans with matrix inclusions only (i.e., 4 of 42 samples), and thresholding values were image specific, based on the relative density of the included tissues, to ensure the best possible segmentation (Fig. S3).

To obtain TBFs from the fossil microCT data, 2D slices of each epiphysis were taken using Avizo 6.1 (Mercury Systems). To do so, the complete 3D TIF stack was reconstructed, and a single slice of trabecular bone (image) was taken from the same anatomical location used with the pQCT scanner protocol (see above and Figs. S2 and S4).

TBF Quantification.

pQCT trabecular quantification. Upon scanning a single bone, an ROI initially was outlined around the entire image, including cortical bone as visualized in the scanner. Then, a Peel mode was used to eliminate concentric rows of voxels from the periosteal surface inward using a user-defined percentage of bone. The peel percentage was set between 60% and 70% in the femoral and humeral heads and between 40% and 50% in the other epiphyseal elements because the amount of trabecular bone vs. cortical bone varies depending on the size and shape of the bone. As noted above, the pQCT uses a calibration standard to convert the raw linear attenuation coefficients into hydroxyapatite-equivalent densities (expressed in milligrams per cubic centimeter).

microCT trabecular quantification. The single 2D images of fossils were each converted into an eight-bit TIF file and were imported into Image J 1.48s (National Institutes of Health). Trabecular bone quantification was performed using the bone-specific plugin Bone J (54). This plugin quantifies TBF as a ratio of mineralized bone area to total area within an ROI. A circular ROI was centered on the center of the epiphysis (Fig. S1). The size of the ROI was standardized by the size of the epiphysis, and the ROI was positioned centrally within the epiphysis to avoid cortical bone. The ROI diameter was defined in the same manner used in the pQCT protocol: 50% of the mediolateral epiphyseal diameter in metacarpal and metatarsal heads, 40% of the mediolateral epiphyseal breadth in the distal tibia, distal radius, and ulnar head, and 60–70% of the epiphyseal diameter in femoral and humeral heads.

Comparison of Scanning Methods. To compare the microCT fossil specimen images directly with those of the pQCT-scanned extant sample, a subset ($n = 25$) of the sample scanned with the pQCT (10 metacarpals, 5 humeri, 5 femora, and 5 metatarsals of chimpanzee skeletons housed at the NMNH) was scanned on the MPI-EVA BIR ACTIS 225/300 microCT scanner using a similar scanning resolution (~30 μm). The size of the ROI was standardized, as was done for fossil hominin specimens, to test for any bias created by using different scanning techniques. Linear regression between the TBF values obtained using microCT and trabecular density using pQCT showed a highly significant correlation (TBF = 0.0006(density) + 0.1567, $r = 0.81$, $P < 0.001$; Fig. S5). This equation was used to predict the microCT-equivalent TBF of extant taxa from their pQCT values (see *SI Materials and Methods* for additional information). A comparison of the 25 chimpanzee specimens scanned with both methods demonstrated that they yielded comparable results (Fig. S6).

Statistical Analyses. Because of the small within-taxon sample sizes for fossils, we used the extant human and chimpanzee means as reference samples to which TBF means, or the TBF value in the case of $n = 1$ for some fossil samples, were compared to show how many SDs a value or sample mean fell from the reference sample. One-way ANOVA with Tukey post-hoc correction was used to identify significant group differences among the extant primates and between pooled fossil *Homo* and *Australopithecus* samples (see *SI Materials and Methods* for additional statistical analyses).

ACKNOWLEDGMENTS. We thank Z. Tsegai and D. Plotzki for help with microCT scanning and the curators at the following institutions for providing access to samples in their care: Tel Aviv University, Musee du Perigord Perigueux, Reihnisches Landesmuseum Bonn, University of the Witwatersrand, National Museums of Kenya, Distong National Museum of Natural History, and the National Museum of Natural History, Smithsonian Institution. MicroCT scans of Sterkfontein fossil material were produced through a collaborative project between the University of the Witwatersrand and the Department of Human Evolution, Max Planck Institute for Evolutionary Anthropology. This research was supported by the Wenner–Gren Foundation for Anthropological Research Wadsworth Fellowship (to H.C.), the Leakey Foundation Baldwin Fellowship (to H.C.), Smithsonian's Peter Buck Postdoctoral Fellowship (to H.C.), and National Science Foundation Grants BCS-0521835 and DGE-0801634 (to B.G.R.).

1. Ruff CB (1988) Hindlimb articular surface allometry in Hominoidea and *Macaca*, with comparisons to diaphyseal scaling. *J Hum Evol* 17(7):687–714.
2. Ruff CB (2002) Long bone articular and diaphyseal structure in old world monkeys and apes. I: Locomotor effects. *Am J Phys Anthropol* 119(4):305–342.
3. Jungers WL (1988) Relative joint size and hominoid locomotor adaptations with implications for the evolution of hominid bipedalism. *J Hum Evol* 17(1-2):247–265.
4. Jungers WL (1990) Scaling of postcranial joint size in hominoid primates. *Gravity, Posture and Locomotion in Primates*, eds Jouffroy FK, Stack MH, Niemitz C (Il Sedicesimo, Florence), pp 87–95.
5. Bramble DM, Lieberman DE (2004) Endurance running and the evolution of *Homo*. *Nature* 432(7015):345–352.
6. Ruff CB, Walker A (1993) Body size and body shape. *The Nariokotome Homo erectus Skeleton*, eds Walker A, Leakey R (Harvard Univ Press, Cambridge, MA), pp 234–265.
7. Pontzer H (2012) Ecological energetics in early *Homo*. *Curr Anthropol* 53(S6):S346–S358.
8. Ruff C (2010) Body size and body shape in early hominins - implications of the Gona pelvis. *J Hum Evol* 58(2):166–178.
9. Richmond BG, Aiello LC, Wood BA (2002) Early hominin limb proportions. *J Hum Evol* 43(4):529–548.
10. Ruff CB, Trinkaus E, Walker A, Larsen CS (1993) Postcranial robusticity in Homo. I: Temporal trends and mechanical interpretation. *Am J Phys Anthropol* 91(1):21–53.
11. Holt BM, et al. Temporal and geographic variation in robusticity. *Skeletal Variation and Adaptation in Europeans: Upper Paleolithic to the Twentieth Century*, ed Ruff CB (Wiley-Blackwell, New York), pp xx.
12. Ruff CB (1998) Evolution of the hominid hip. *Primate Locomotion: Recent Advances*, eds Strasser E, Rosenberger A, McHenry H, Fleagle J (Plenum, Davis, CA), pp 449–469.
13. Marchi D, Sparacello V, Shaw C (2011) Mobility and lower limb robusticity of a pastoralist Neolithic population from north-western Italy. *Human Bioarchaeology of the Transition to Agriculture*, eds Pinhasi R, Stock JT (Wiley-Blackwell, New York), pp 317–346.
14. Ruff CB, et al. (2006) Body size, body proportions, and mobility in the Tyrolean "Iceman". *J Hum Evol* 51(1):91–101.
15. Holt BM (2003) Mobility in Upper Paleolithic and Mesolithic Europe: Evidence from the lower limb. *Am J Phys Anthropol* 122(3):200–215.
16. Trinkaus E, Ruff CB (2012) Femoral and tibial diaphyseal cross-sectional geometry in Pleistocene *Homo*. *PaleoAnthropology* 2012:13–62.
17. Cowgill LW (2010) The ontogeny of Holocene and Late Pleistocene human postcranial strength. *Am J Phys Anthropol* 141(1):16–37.
18. Ruff C, Holt B, Trinkaus E (2006) Who's afraid of the big bad Wolff?: "Wolff's law" and bone functional adaptation. *Am J Phys Anthropol* 129(4):484–498.
19. Shaw CN, Stock JT (2013) Extreme mobility in the Late Pleistocene? Comparing limb biomechanics among fossil *Homo*, varsity athletes and Holocene foragers. *J Hum Evol* 64(4):242–249.
20. Frayer DW (1981) Body size, weapon use and natural selection in the European Upper Paleolithic and Mesolithic. *Am Anthropol* 83(1):57–73.
21. Stock JT (2006) Hunter-gatherer postcranial robusticity relative to patterns of mobility, climatic adaptation, and selection for tissue economy. *Am J Phys Anthropol* 131(2):194–204.
22. Macintosh AA, Pinhasi R, Stock JT (2014) Lower limb skeletal biomechanics track long-term decline in mobility across ~6150 years of agriculture in central Europe. *J Arch Sci* 52:376–390.
23. Pettersson U, Nilsson M, Sundh V, Mellström D, Lorentzon M (2010) Physical activity is the strongest predictor of calcaneal peak bone mass in young Swedish men. *Osteoporos Int* 21(3):447–455.
24. Stock JT, Pfeiffer SK (2004) Long bone robusticity and subsistence behaviour among Later Stone Age foragers of the forest and fynbos biomes of South Africa. *J Arch Sci* 31(7):999–1013.
25. Trinkaus E, Churchill SE, Ruff CB (1994) Postcranial robusticity in Homo. II: Humeral bilateral asymmetry and bone plasticity. *Am J Phys Anthropol* 93(1):1–34.
26. Ruff CB (2005) Mechanical determinants of bone form: Insights from skeletal remains. *J Musculoskelet Neuronal Interact* 5(3):202–212.
27. Schackelford LL (2007) Regional variation in the postcranial robusticity of late Upper Paleolithic humans. *Am J Phys Anthropol* 133(1):655–68.
28. Ryan TM, Ketcham RA (2002b) Femoral head trabecular bone structure in two omomyid primates. *J Hum Evol* 43(2):241–263.
29. Robson Brown KA, Davies EN, McNally DS (2002) The angular distribution of vertebral trabeculae in modern humans, chimpanzees and the Kebara 2 Neanderthal. *J Hum Evol* 43(2):189–205.
30. Griffin NL (2008) Bone architecture of the hominin second proximal pedal phalanx: A preliminary investigation. *J Hum Evol* 54(1):162–168.
31. Scherf H, Harvati K, Hublin J-J (2013) A comparison of proximal humeral cancellous bone of great apes and humans. *J Hum Evol* 65(1):29–38.
32. Tsegai ZJ, et al. (2013) Trabecular bone structure correlates with hand posture and use in hominoids. *PLoS ONE* 8(11):e78781–e78781.
33. Zeininger A, Richmond BG, Hartman G (2011) Metacarpal head biomechanics: A comparative backscattered electron image analysis of trabecular bone mineral density in *Pan troglodytes, Pongo pygmaeus*, and *Homo sapiens*. *J Hum Evol* 60(6):703–710.
34. Ruff C (2008) Femoral/humeral strength in early African *Homo erectus*. *J Hum Evol* 54(3):383–390.
35. Maga M, Kappelman J, Ryan TM, Ketcham RA (2006) Preliminary observations on the calcaneal trabecular microarchitecture of extant large-bodied hominoids. *Am J Phys Anthropol* 129(3):410–417.
36. Griffin NL, et al. (2010) Comparative forefoot trabecular bone architecture in extant hominids. *J Hum Evol* 59(2):202–213.
37. Ruff CB, Larsen CS (1990) Postcranial biomechanical adaptations to subsistence changes on the Georgia Coast. *Anthropol Pap Am Mus Nat Hist* 68:94–120.
38. Ruff CB, Larsen CS (2001) Reconstructing behavior in Spanish Florida: The biomechanical evidence. *Bioarchaeology of Spanish Florida: The Impact of Colonialism*, ed Larsen CS (Univ Press of Florida, Gainesville, FL), pp 113–145.
39. Bridges PS (1989) Changes in activities with the shift to agriculture in the southeastern United States. *Curr Anthropol* 30(3):385–394.
40. Pearson OM (2000) Postcranial remains and the origin of modern humans. *Evol Anthropol* 9(6):229–247.
41. Lieberman DE (1996) How and why humans grow thin skulls: Experimental evidence for systemic cortical robusticity. *Am J Phys Anthropol* 101(2):217–236.
42. Keaveny TM, Morgan EF, Niebur GL, Yeh OC (2001) Biomechanics of trabecular bone. *Annu Rev Biomed Eng* 3:307–333.
43. Morgan EF, Bayraktar HH, Keaveny TM (2003) Trabecular bone modulus-density relationships depend on anatomic site. *J Biomech* 36(7):897–904.
44. Fajardo RJ, Müller R, Ketcham RA, Colbert M (2007) Nonhuman anthropoid primate femoral neck trabecular architecture and its relationship to locomotor mode. *Anat Rec (Hoboken)* 290(4):422–436.
45. Ryan TM, Walker A (2010) Trabecular bone structure in the humeral and femoral heads of anthropoid primates. *Anat Rec (Hoboken)* 293(4):719–729.
46. Pontzer H, et al. (2006) Trabecular bone in the bird knee responds with high sensitivity to changes in load orientation. *J Exp Biol* 209(Pt 1):57–65.
47. Barak MM, Lieberman DE, Hublin JJ (2011) A Wolff in sheep's clothing: Trabecular bone adaptation in response to changes in joint loading orientation. *Bone* 49(6):1141–1151.
48. Garn SM, Guzmán MA, Wagner B (1969) Subperiosteal gain and endosteal loss in protein-calorie malnutrition. *Am J Phys Anthropol* 30(1):153–155.
49. Eaton SB, Nelson DA (1991) Calcium in evolutionary perspective. *Am J Clin Nutr* 54(1, Suppl):281S–287S.
50. Cohen MN, Armelagos GJ (1984) *Paleopathology at the origins of agriculture* (Academic Press, New York).
51. Cohen MN, Crane-Kramer GMM, eds (2007) *Ancient Health: Skeletal indicators of agricultural and economic intensification* (University Press of Florida, Gainesville).
52. Augat P, Gordon CL, Lang TF, Iida H, Genant HK (1998) Accuracy of cortical and trabecular bone measurements with peripheral quantitative computed tomography (pQCT). *Phys Med Biol* 43(10):2873–2883.
53. Scherf H, Tilgner R (2009) A new high-resolution computed tomography (CT) segmentation method for trabecular bone architectural analysis. *Am J Phys Anthropol* 140(1):39–51.
54. Doube M, et al. (2010) BoneJ: Free and extensible bone image analysis in ImageJ. *Bone* 47(6):1076–1079.

Supporting Information

Chirchir et al. 10.1073/pnas.1411696112

SI Materials and Methods

Samples.

Extant primates. The Terry collection contains skeletons of late 19th century and early 20th century working-class Americans of European descent (only one ancestry was selected) from St. Louis Hospital (1). The Puye collection is a late prehistoric archaeological sample of people who inhabited the northern portion of the Pajarito plateau, New Mexico, between ∼900 and 1300 AD (2). The Puye subsisted by farming in the lowlands and returning to their dwellings in the plateau settlements, suggesting that they engaged in regular levels of activity that exceeded those of most individuals represented in the industrial working-class Terry Collection. A *t* test between the TBFs of the two recent modern human samples in each element revealed no significant differences ($P > 0.05$), and consequently those two samples were pooled.

Anatomical locations of scans. Each anatomical element was positioned systematically to obtain scans of homologous regions at the center of the joint. The medial-lateral breadth of femoral and humeral heads was measured, and half of the breadth was used to identify the position in which an image slice orthogonal to the axis of the neck would be taken (Fig. S2 *A* and *B*; breadth and height definitions are provided in figure captions). For the distal tibia and distal radius the superior–inferior height of the epiphysis was measured, and half of the height was identified as the position where a transverse slice would be taken (Fig. S2 *C* and *D*). Finally, for the proximal ulna and for the metacarpal and metatarsal heads, half of the superior–inferior height of each element (i.e., the proximal ulna and the metacarpal and metatarsal heads) was identified as the location of the image slice (Fig. S2 *E* and *F*).

Further Methods. Not all postcranial elements were preserved for each fossil taxon (Table 1 and Table S2). In particular, although the extant sample quantified TBF only in the third metacarpal (Mc3) and metatarsal (Mt3), metacarpals from all manual/pedal rays were used, depending on availability in the fossil sample. The loading of the different rays varies across the hand/foot, and this variation may be reflected in the TBF, because it can be reflected in the cross-sectional geometry of diaphyses (3). Therefore, we tested variation in TBF across chimpanzee and recent modern human first, third, and fifth metacarpals (Mc1, Mc3, and Mc5, respectively). We found no significant difference in TBF between Mc3 and Mc5 ($P = 0.139$ in $n = 10$ chimpanzees, and $P = 0.48$ in $n = 10$ recent humans). Mc1 had significantly higher TBF, but the relative differences between chimpanzees and recent modern humans remained the same. Therefore, the pattern of relative densities between taxa remains robust.

Data are not currently available to assess variation in metatarsals among rays within individuals. Therefore, we must make the assumption that the variation among rays within individuals is less than the variation between species. We believe that this assumption is reasonable, based on the limited data available, because, although density may differ significantly between metatarsal 1 (Mt1) and metatarsal 5 (Mt5), the fossil metatarsal with the highest value is the early modern human (Oberkassel) Mt5 (TBF = 0.455). The Swartkraans specimens include an Mt1 specimen (SK1813) with a similarly high value (TBF = 0.455) and another Mt1 (SKX 5017) with the lowest of the fossil values (TBF = 0.288). Thus, high and low TBF values are observed within Mt1 and Mt5 fossil specimens. Furthermore, the metatarsals follow the same pattern as the other lower limb elements, and the overall pattern observed in the lower limb (Fig. 3*B*) remains robust if the metatarsal data are excluded.

In addition, this study included Neandertal 1, which is known to have a pathological left arm (4). The nonpathological right humerus, radius, and ulna were included in this analysis, and although they may present hypertrophied cortical structure (4), the TBF values were similar to, and in fact were slightly lower than, those of the other Neandertal specimens. For example, the trabecular fraction of the Neandertal 1 right humeral epiphyses (0.245) is similar to that of the other Neandertal specimens (with a mean of 0.270). Because the Neandertal 1 values are in fact slightly lower (e.g., a TBF density of 0.251 in the distal radius), rather than higher, as one might expect if there was increased unilateral use of the nonpathological arm, we see no evidence to suggest that the trabecular density in Neandertal 1 is abnormal for this group. The Neandertal sample consistently has generally high TBF levels.

Oberkassel 1 also has some evidence of posttraumatic changes in the upper limb, including ulnar fracture and coracoclavicular ossification (5), but recent reevaluation suggests that the trauma did not influence overall arm hypertrophy (6). Moreover, the trauma in the Oberkassel 1 arm would not impact the trabecular bone in the femur, which has a TBF value (0.349) comparable to that in the Qafzeh 9 femur (0.40). We originally examined additional fossils but could not include them because they could not be measured reliably (e.g., the Skhul IV femoral head and distal tibia are filled with matrix that obscure trabecular struts). A larger sample of early modern humans would help clarify when and in what specific context trabecular density decreased in modern humans.

Additional Statistical Analyses. A *t* test between male and female humerus and femur TBF within each recent modern human population did not reveal significant differences ($P > 0.05$) (Table S4), and therefore sexes were combined. In addition, the TBF in the right and left arms (i.e., in the humeral heads) was quantified in a subsample of both recent modern human populations. A *t* test did not reveal any significant differences ($P > 0.05$) in this comparison, either (Tables S1 and S4).

1. Hunt DR, Albanese J (2005) History and demographic composition of the Robert J. Terry anatomical collection. *Am J Phys Anthropol* 127(4):406–417.
2. Hewett EL (1953) *Ancient Life in the American Southwest* (Biblo and Tannen, New York).
3. Griffin NL, Richmond BG (2005) Cross-sectional geometry of the human forefoot. *Bone* 37(2):253–260.
4. Trinkaus E, Churchill SE, Ruff CB (1994) Postcranial robusticity in Homo. II: Humeral bilateral asymmetry and bone plasticity. *Am J Phys Anthropol* 93(1):1–34.
5. Churchill SE, Formicola V (1997) A case of marked bilateral asymmetry in the upper limbs of an Upper Palaeolithic male from Barma Grande (Liguria), Italy. *Int J Osteoarchaeol* 7(1):18–38.
6. Trinkaus E, The appendicular skeletal remains of Oberkassel 1 and 2. *Oberkassel 1914-2014. 100 Years of Research on the Late Glacial Burial*, eds Giemsch L, Schmitz RW (Rheinische Ausgrabungen. Rheinische Landesmuseum, Bonn).

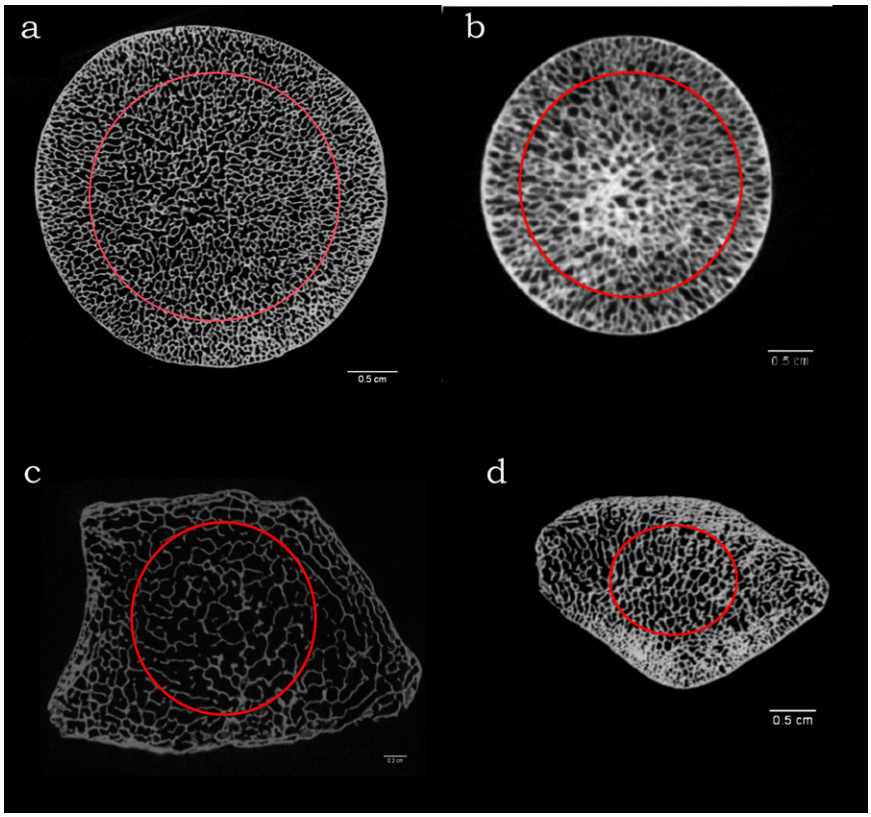

Fig. S1. The ROI in which trabecular fraction was quantified is outlined in red. (*A* and *B*) Chimpanzee humeral head (*A*) and femoral head (*B*). (*C* and *D*) Neanderthal distal radius (*C*) and proximal ulna (*D*).

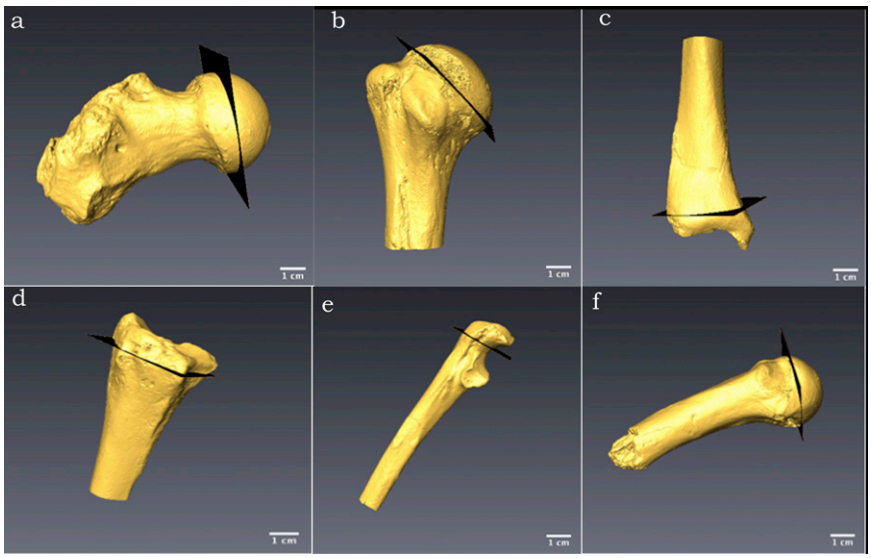

Fig. S2. Images demonstrating the position and plane of the 2D slice in each anatomical element, taken either at the location of pQCT scanning or at a single slice derived from a 3D volume (e.g., in fossil specimens). (*A* and *B*) In the femoral head, the medio-lateral breadth is the breadth of the articular surface from the lateral and central-most point of the head to the medial and central-most point of the humeral head (*A*) and is the breadth of the head from the lateral-most point (including the lesser tuberosity) to the medial and central-most point (*B*). (*C* and *D*) In the distal tibia, the superior–inferior height is measured on the lateral (fibular notch side) surface of the epiphysis, which is the depth of the articulation with the fibula/distal radius, (C) and is measured on the medial side, which is the depth of the articular surface with ulna (*D*). (*E*) In the proximal ulna, the superior–inferior height is the height of olecranon process from the most superior border to the center of the trochlear notch. (*F*) In the metacarpal/metatarsal, the proximal–distal length is measured as the superior–inferior breadth of the head from the central and distal-most point of the head to the proximal extent of the articular surface.

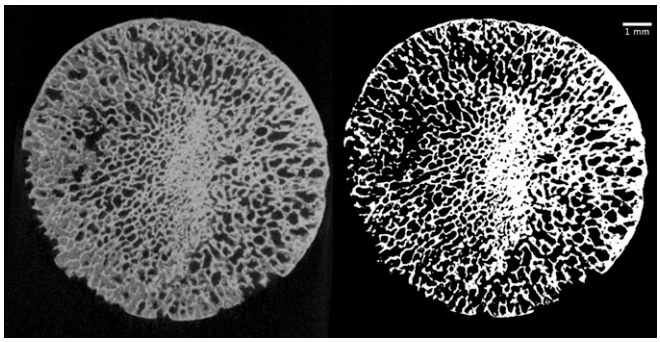

Fig. S3. An example of the segmentation of one of the four fossil specimens that needed to have matrix removed from the trabecular bone. Here, the 2D slice of the *Australopithecus* sp. specimen KNM-ER 738AB is shown unsegmented (*Left*) and segmented (*Right*), using the Ray-casting algorithm.

Fig. S4. Positioning of the femoral head in the pQCT scanner, shown as an example of the pQCT setup that ensured homologous scanning of the same position and plane in each specimen.

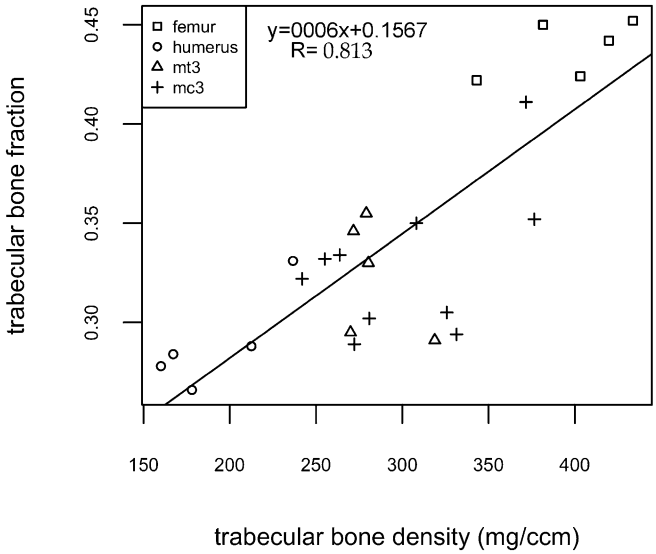

Fig. S5. Plot of the trabecular fraction (bone pixels/total pixels) in chimpanzee femoral ($n = 5$), humeral ($n = 5$), metatarsal (mt3; $n = 5$), and metacarpal (mc3; $n = 10$) heads of specimens scanned at the MPI using microCT, against pQCT density measured at the NMNH. The same individuals were scanned with both scanners to establish the relationship between these measures. The linear regression shown here was significant ($P < 0.001$; $r^2 = 0.66$) and was used to convert pQCT densities (most of the extant samples) into micro-CT trabecular fraction (most of the fossil samples).

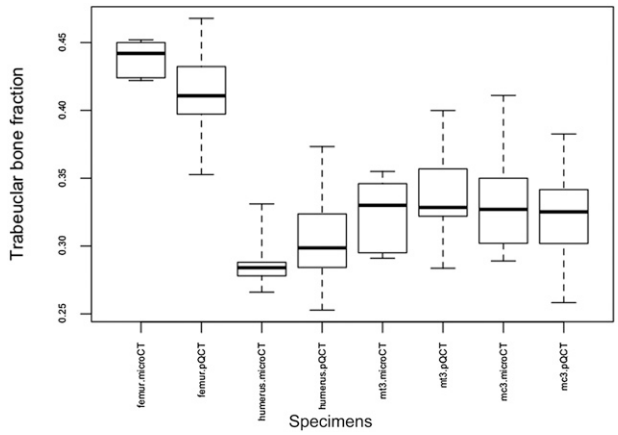

Fig. S6. A plot of trabecular measurements in the 25 chimpanzee skeletal specimens scanned using both methods shows that the two methods yield comparable results. The plot illustrates the MPI microCT-derived TBF measurements and the TBF estimates derived from the regression (Fig. S5) based on the pQCT density measurements (at the NMNH).

Table S1. Extant samples included in this study

	Recent *Homo sapiens*			*Pan troglodytes*		*Pongo pygmaeus*		*Papio anubis*	
Element	Terry, *n* male/*n* female	Puye, *n* male/*n* female	Total	*n* male/*n* female	Total	*n* male/*n* female	Total	*n* male/*n* female	Total
Upper limb									
Proximal humerus	11M/9F*	10M/8F*	38	8M/9F	17	5M/10F	15	9M/6F/2 unknown	17
Proximal ulna	11M/9F	10M/8F	38	8M/9F	17	6M/10F	16	9M/6F/2 unknown	17
Distal radius	11M/9F	10M/8F	38	8M/9F	17	6M/10F	16	9M/6F/2 unknown	17
Proximal Mc3	10M/10F	5M/5F	30	8M/9F	17	6M/10F	16	6M/5F/1 unknown	12
Lower limb									
Proximal femur	11M/9F	10M/8F	38	8M/9F	17	6M/10F	16	9M/7F/2 unknown	18
Distal tibia	11M/9F	10M/8F	38	8M/9F	17	6M/10F	16	9M/7F/2 unknown	18
Proximal Mt3	11M/9F	10M/5F	35	8M/9F	17	6M/10F	16	9M/6F/2 unknown	17

All specimens are housed at the National Museum of Natural History. Terry right humeri: $n = 10$, left humeri: $n = 10$; Puye right humeri: $n = 10$, left humeri: $n = 9$.

*Left and right arms were sampled.

Table S2. Fossil hominin samples used in this analysis

Taxon	Specimen	Side	Sex	Collection	TBF
Proximal humerus (n = 5)					
Australopithecus africanus	StW 328	R	?	WITS	0.463
Homo neanderthalensis	Kebara 2	L	M	TAU	0.281
Homo neanderthalensis	Le Regourdou 1	R	?	MAAP	0.295
Homo neanderthalensis	Neanderthal 1 322.09	R	?	LVRB	0.245
Early modern *Homo sapiens*	Oberkassel 998.56	L	M	LVRB	0.260
Proximal ulna (n = 7)					
Australopithecus africanus	StW 431	R	?	WITS	0.573
Australopithecus africanus	StW 398	L	?	WITS	0.484
Australopithecus africanus	StW 380	R	?	WITS	0.403
Australopithecus africanus	StW 113	L	?	WITS	0.434
Homo neanderthalensis	Kebara 2	R	M	TAU	0.488
Homo neanderthalensis	Neanderthal 1 322.11	R	?	LVRB	0.464
Early modern *Homo sapiens*	Oberkassel 999.31	R	F	LVRB	0.332
Distal radius (n = 3)					
Paranthropus robustus/early *Homo*	SKX 3602	R	?	Ditsong	0.296
Homo neanderthalensis	Kebara 2	R	M	TAU	0.517
Homo neanderthalensis	Neanderthal 1 332.10	R	?	LVRB	0.251
Proximal metacarpals (n = 10)					
Australopithecus africanus	StW 418 (Mc1)*	R	?	WITS	0.339
Australopithecus africanus	StW 382 (Mc2)	L	?	WITS	0.284
Australopithecus africanus	StW 394 (Mc3)	L	?	WITS	0.308
Australopithecus africanus	StW 292 (Mc4)	R	?	WITS	0.283
Australopithecus africanus	StW 552 (Mc4)	R	?	WITS	0.318
Paranthropus robustus/early *Homo*	SK 84 (Mc1)*	L	?	Ditsong	0.242
Paranthropus robustus/early *Homo*	SKX 5020 (Mc1)*	R	?	Ditsong	0.345
Homo neanderthalensis	Kebara 2 (Mc3)	R	M	TAU	0.244
Early modern *Homo sapiens*	Qafzeh 9 (Mc3)	R	F	TAU	0.393
Early modern *H. sapiens*	Oberkassel 998.72 (Mc2)	R	M	LVRB	0.255
Proximal femur (n = 8)					
Australopithecus sp.	KNM-ER 738AB*	R	?	KNM	0.436
Australopithecus africanus	StW 527	?	?	WITS	0.527
Australopithecus africanus	StW 311	R	?	WITS	0.475
Australopithecus africanus	StW 403	L	?	WITS	0.366
Homo neanderthalensis	Neanderthal 1 322.15	L	?	LVRB	0.424
Homo neanderthalensis	Neanderthal 1 322.16	R	?	LVRB	0.367
Early modern *Homo sapiens*	Qafzeh 9	L	F	TAU	0.400
Early modern *Homo sapiens*	Oberkassel 998.66	R	M	LVRB	0.349
Distal tibia (n = 5)					
Australopithecus africanus	StW 181	L	?	Ditsong	0.378
Australopithecus africanus	StW 358	L	?	Ditsong	0.524
Australopithecus africanus	StW 389	R	?	Ditsong	0.417
Early modern *Homo sapiens*	Oberkassel 998.75	L	M	LVRB	0.342
Early modern *H. sapiens*	Oberkassel 999.37	R	F	LVRB	0.245
Proximal metatarsal (n = 4)					
Paranthropus robustus/early *Homo*	SKX 33380 (Mt5)	L	?	Ditsong	0.343
Paranthropus robustus/early *Homo*	SK 1813 (Mt1)	R	?	Ditsong	0.435
Paranthropus robustus/early *Homo*	SKX 5017 (Mt1)	R	?	Ditsong	0.288
Early modern *Homo sapiens*	Oberkassel D998.71 (Mt5)	R	M	LVRB	0.455

KNM, Kenya National Museum; LVRB, Reihnisches Landesmuseum Bonn; MAAP, Musee du Perigord Perigueux; TAU, Tel Aviv University; WITS, University of the Witwatersrand.
*Fossil specimens that required segmentation of trabeculae from matrix (n = 4 specimens out of a total of 42 samples).

Table S3. Tukey pairwise comparisons between recent modern humans and other extant primates and between fossil *Homo* (excluding recent modern humans) and australopiths in pooled trabecular fractions for upper limb elements and pooled lower limb elements

Element	Recent humans vs. chimpanzees	Recent humans vs. orangutans	Recent humans vs. baboons	Fossil *Homo* vs. australopiths
Lower limb	$P < 0.0001$	$P < 0.0001$	$P < 0.0001$	$P = 0.18$
Upper limb	$P < 0.0001$	$P < 0.0001$	$P < 0.0001$	$P = 0.17$

Recent modern humans have significantly lower trabecular fractions, and australopiths and fossil *Homo* show a nonsignificant difference in pooled values.

Table S4. Student *t* test for sexual dimorphism and bilateral asymmetry

Trait	Collection	Femur	Humerus
Sexual dimorphism (males vs. females)	Terry	$P = 0.48$	$P = 0.07$
	Puye	$P = 0.08$	$P = 0.43$
Bilateral asymmetry in the arm	Terry	—	$P = 0.27$
	Puye	—	$P = 0.37$